

Ternary Antimonides $RE_4T_7Sb_6$ ($RE = \text{Gd-Lu}$; $T = \text{Ru, Rh}$) with Cubic $U_4\text{Re}_7\text{Si}_6$ -type Structure

Inga Schellenberg, Ute Ch. Rodewald, Christian Schwickert, Matthias Eul, and Rainer Pöttgen

Institut für Anorganische und Analytische Chemie, Universität Münster, Corrensstrasse 30, 48149 Münster, Germany

Reprint requests to R. Pöttgen. E-mail: pottgen@uni-muenster.de

Z. Naturforsch. **2013**, 68b, 971–978 / DOI: 10.5560/ZNB.2013-3181

Received July 3, 2013

The ternary antimonides $RE_4T_7Sb_6$ ($RE = \text{Gd-Lu}$; $T = \text{Ru, Rh}$) have been synthesized from the elements by arc-melting and subsequent annealing in an induction furnace. The samples have been characterized by powder X-ray diffraction. Four structures were refined on the basis of single-crystal X-ray diffractometer data: $U_4\text{Re}_7\text{Si}_6$ type, space group $Im\bar{3}m$ with $a = 862.9(2)$ pm, $wR2 = 0.0296$, 163 F^2 values for $\text{Er}_4\text{Ru}_7\text{Sb}_6$; $a = 864.1(1)$ pm, $wR2 = 0.1423$, 153 F^2 values for $\text{Yb}_4\text{Ru}_7\text{Sb}_6$; $a = 872.0(2)$ pm, $wR2 = 0.0427$, 172 F^2 values for $\text{Tb}_4\text{Rh}_7\text{Sb}_6$; and $a = 868.0(2)$ pm, $wR2 = 0.0529$, 154 F^2 values for $\text{Er}_4\text{Rh}_7\text{Sb}_6$, with 10 variables per refinement. The structures have $T1@\text{Sb}_6$ octahedra and slightly distorted $RE@T_2\text{Sb}_6$ cuboctahedra as building units. The distorted cuboctahedra are condensed *via* all trapezoidal faces, and this network leaves octahedral voids for the $T1$ atoms. The ruthenium-based series of compounds was studied by temperature-dependent magnetic susceptibility measurements. $\text{Lu}_4\text{Ru}_7\text{Sb}_6$ is Pauli-paramagnetic. The antimonides $RE_4\text{Ru}_7\text{Sb}_6$ with $RE = \text{Dy, Ho, Er, and Tm}$ show Curie-Weiss paramagnetism. Antiferromagnetic ordering occurs at 10.0(5), 5.1(5) and 4.0(5) K for $\text{Dy}_4\text{Ru}_7\text{Sb}_6$, $\text{Ho}_4\text{Ru}_7\text{Sb}_6$ and $\text{Er}_4\text{Ru}_7\text{Sb}_6$, respectively, while $\text{Tm}_4\text{Ru}_7\text{Sb}_6$ remains paramagnetic. $\text{Yb}_4\text{Ru}_7\text{Sb}_6$ is an intermediate-valent compound with a reduced magnetic moment of 3.71(1) μ_B per Yb as compared to 4.54 μ_B for a free Yb^{3+} ion.

Key words: Antimonides, Crystal Structure, Magnetic Properties

Introduction

The discovery of superconductivity in potassium-doped BaFe_2As_2 with a maximum T_C of 38 K [1, 2] led to a true renaissance of research in the field of pnictides with BaAl_4 -related structures [3, 4]. Besides diverse ternary ordering variants [5], many solid solutions $RE_{1-x}\text{RE}'_xT_2X_2$ and $RET_{2-x}T'_xX_2$ ($RE = \text{rare earth element}$; $T = \text{transition metal}$; $X = \text{element of the 3rd, 4th, or 5th main group}$) have been studied [6, 7]. Especially in the case of cerium compounds the solid solutions $\text{La}_{1-x}\text{Ce}_xT_2X_2$ have been investigated with respect to cerium magnetism. The solid solutions $RET_{2-x}T'_xX_2$ allow for a variation of the valence electron concentration and thus a change in the magnetic properties.

Many BaAl_4 -related structures show formation of distinct vacancies $RET_{2-x}X_2$ or RET_2X_{2-x} to release structural strain. In many cases only the subcell struc-

tures have been reported, and precise reinvestigations have shown the formation of ordered superstructures, such as $\text{Ce}_3\text{Pd}_6\text{Sb}_5 \equiv \text{CePd}_2\text{Sb}_{1.66}$ [8, 9], $\text{Dy}_3\text{Co}_6\text{Sn}_5 \equiv \text{DyCo}_2\text{Sn}_{1.66}$ [10], $\text{Eu}_2\text{Au}_2\text{Sn}_5 \equiv \text{EuAuSn}_{2.5}$ [5], $\text{Yb}_3\text{Au}_{5.5}\text{Ga}_{5.5} \equiv \text{YbAu}_{1.83}\text{Ga}_{1.83}$ [11], $\text{Yb}_5\text{Cu}_{11}\text{Sn}_8 \equiv \text{YbCu}_{2.20}\text{Sn}_{1.60}$ [12], or $\text{Ce}_8\text{Rh}_{17}\text{Sb}_{14} \equiv \text{CeRh}_{2.13}\text{Sb}_{1.75}$ [13].

Some unique compounds with composition close to 1-2-2 have been reported, however, with distinctly different structures. In $\text{Ca}_4\text{Ir}_8\text{P}_7 \equiv \text{CaIr}_2\text{P}_{1.75}$ [14] and $\text{La}_4\text{Rh}_8\text{P}_9 \equiv \text{LaRh}_2\text{P}_{2.25}$ [15] only parts of the structure resemble the ThCr_2Si_2 respectively CaBe_2Ge_2 types (ordered BaAl_4 versions). This is different for the larger family of $U_4\text{Re}_7\text{Si}_6 \equiv \text{URe}_{1.75}\text{Si}_{1.50}$ compounds which display completely different crystal chemistry. Instead of the tetrahedral transition metal coordination in the ThCr_2Si_2 phases one observes octahedral besides tetrahedral coordination in the $U_4\text{Re}_7\text{Si}_6$ -type structure. In the course of our systematic studies of

structure-property relationships of ternary antimonides with BaAl₄-related structures [9, 13, 16, 17] we obtained the series of cubic antimonides $RE_4Ru_7Sb_6$ ($RE = Tb-Lu$) and $RE_4Rh_7Sb_6$ ($RE = Gd-Lu$) with U₄Re₇Si₆-type structure. The structure and properties of these phases are reported herein.

Experimental

Synthesis

Starting materials for the syntheses of the $RE_4Ru_7Sb_6$ and $RE_4Rh_7Sb_6$ samples were sublimed rare earth pieces (Smart elements or Johnson Matthey), ruthenium and rhodium powder (Heraeus or Allgemeine Pforzheim), and antimony lumps (Johnson Matthey), all with stated purities better than 99.9 %. Polycrystalline samples are available directly *via* arc-melting [18] of the elements (pieces of the rare earth metal, a cold-pressed pellet of ruthenium (rhodium) and pieces of the antimony lumps) under an argon atmosphere of *ca.* 700 mbar. The argon was purified over titanium sponge (900 K), silica gel, and molecular sieves. The product buttons were remelted three times to ensure homogeneity. The total weight losses after the melting procedure were always smaller than 0.5 %. The buttons were subsequently sealed in evacuated quartz tubes and annealed in a water-cooled sample chamber of an induction furnace (Hüttinger Elektronik, Freiburg, type TIG 1.5/300) [19] at *ca.* 1370 K for one hour. The resulting $RE_4Ru_7Sb_6$ and $RE_4Rh_7Sb_6$ samples are silvery with metallic luster. They are stable in air over months.

EDX data

Semiquantitative EDX analyses of the single crystals studied on the diffractometer were carried out in variable

Table 1. Lattice parameters (Guinier powder data) of ternary antimonides with U₄Re₇Si₆-type structure.

Compound	a (pm)	V (nm ³)
Tb ₄ Ru ₇ Sb ₆	868.1(1)	0.6542
Dy ₄ Ru ₇ Sb ₆	866.5(1)	0.6506
Ho ₄ Ru ₇ Sb ₆	864.5(1)	0.6461
Er ₄ Ru ₇ Sb ₆	864.1(1)	0.6452
Tm ₄ Ru ₇ Sb ₆	862.1(1)	0.6407
Yb ₄ Ru ₇ Sb ₆	862.9(2)	0.6425
Lu ₄ Ru ₇ Sb ₆	860.6(1)	0.6374
Gd ₄ Rh ₇ Sb ₆	875.7(1)	0.6715
Tb ₄ Rh ₇ Sb ₆	872.0(2)	0.6631
Dy ₄ Rh ₇ Sb ₆	870.5(1)	0.6596
Ho ₄ Rh ₇ Sb ₆	869.2(1)	0.6567
Er ₄ Rh ₇ Sb ₆	868.0(2)	0.6540
Tm ₄ Rh ₇ Sb ₆	865.4(1)	0.6481
Yb ₄ Rh ₇ Sb ₆ ^a	865.9(2)	0.6492
Yb ₄ Rh ₇ Sb ₆ ^b	865.24(2)	0.6478
Lu ₄ Rh ₇ Sb ₆	863.3(1)	0.6434

^a Data from ref. [22]; ^b data from ref. [26]

pressure mode with a Zeiss EVO[®] MA10 scanning electron microscope with the rare earth trifluorides, Ru, Rh, and Sb as standards. The experimentally observed average compositions were close to the ideal ones. No impurity elements were detected.

X-Ray diffraction

The polycrystalline $RE_4Ru_7Sb_6$ and $RE_4Rh_7Sb_6$ samples were characterized by Guinier patterns (imaging plate detector, Fujifilm BAS-1800) with Cu $K_{\alpha 1}$ radiation and α -quartz ($a = 491.30$, $c = 540.46$ pm) as an internal standard. The cubic lattice parameters (Table 1) were refined by a standard least-squares routine. To ensure correct indexing, we compared the experimental patterns with calculated ones [20].

Empirical formula	Er ₄ Ru ₇ Sb ₆	Yb ₄ Ru ₇ Sb ₆	Tb ₄ Rh ₇ Sb ₆	Er ₄ Rh ₇ Sb ₆
Formula weight, g mol ⁻¹	2107.03	2130.15	2086.55	2119.91
Unit cell dimensions	Table 1	Table 1	Table 1	Table 1
Calculated density, g cm ⁻³	10.85	11.01	10.45	10.77
Crystal size, μm^3	15 × 20 × 25	20 × 20 × 25	20 × 30 × 30	15 × 20 × 20
Transm. ratio (min / max)	0.193 / 0.492	0.118 / 0.298	0.146 / 0.373	0.248 / 0.747
Abs. coefficient, mm ⁻¹	45.9	49.1	41.4	46.0
$F(000)$, e	1772	1788	1762	1786
θ range for data coll., deg	3–33	3–35	3–35	3–34
Range in hkl	±13, ±13, ±13	±13, ±13, ±13	±13, ±13, ±13	±13, ±13, ±13
Total no. of reflections	3071	4568	5167	4599
Independent reflections / R_{int}	153 / 0.1559	163 / 0.1229	172 / 0.0343	154 / 0.1727
Reflections with $I > 2\sigma(I)$ / R_{σ}	105 / 0.0555	128 / 0.0321	158 / 0.0123	136 / 0.0494
Data / parameters	153 / 10	163 / 10	172 / 10	154 / 10
Goodness-of-fit on F^2	0.950	0.909	1.165	1.251
$R1$ / $wR2$ for $I > 2\sigma(I)$	0.0509 / 0.1310	0.0183 / 0.0277	0.0198 / 0.0414	0.0275 / 0.0496
$R1$ / $wR2$ for all data	0.0731 / 0.1423	0.0296 / 0.0296	0.0249 / 0.0427	0.0394 / 0.0529
Extinction coefficient	0.00042(17)	0.00042(4)	0.00075(6)	0.00018(8)
Largest diff. peak / hole, e Å ⁻³	3.20 / -4.96	2.86 / -1.96	1.78 / -1.69	1.83 / -1.95

Table 2. Crystal data and structure refinement of Tb₄Rh₇Sb₆, Er₄Rh₇Sb₆, Er₄Ru₇Sb₆, and Yb₄Ru₇Sb₆. Space group $Im\bar{3}m$; $Z = 2$.

Suitable single crystals were selected from the crushed $Er_4Ru_7Sb_6$, $Yb_4Ru_7Sb_6$, $Tb_4Rh_7Sb_6$, and $Er_4Rh_7Sb_6$ samples, glued to thin quartz fibers using beeswax and studied on a Buerger camera (using white Mo radiation) to check their quality. The data sets were measured on a Stoe IPDS-II image plate system (graphite-monochromatized $MoK\alpha$ radiation; $\lambda = 71.073$ pm) in oscillation mode. Numerical absorption corrections were applied to the data sets. Details about the data collections and the crystallographic parameters are summarized in Table 2.

Structure refinements

The four data sets showed body-centred cubic lattices and no further systematic extinctions in agreement with our previous work on $Yb_4Rh_7Ge_6$ [21] and $Yb_4Rh_7Sb_6$ [22]. The atomic parameters of the antimonide were taken as starting values, and the structures were refined with anisotropic displacement parameters for all atoms using SHELXL-97 (full-matrix least-squares on F^2) [23, 24]. To check for deviations from the ideal compositions, the occupancy parameters were refined in separate series of least-squares cycles for all data sets. The sites were fully occupied within two standard deviations. The final difference Fourier synthesis revealed no residual peaks. The refined atomic positions, equivalent isotropic displacement parameters, and interatomic distances are given in Tables 3 and 4.

Further details of the crystal structure investigation may be obtained from Fachinformationszentrum Karlsruhe, 76344 Eggenstein-Leopoldshafen, Germany (fax: +49-7247-808-666; e-mail: crysdata@fiz-karlsruhe.de, http://www.fiz-karlsruhe.de/request_for_deposited_data.html) on quoting the deposition numbers CSD-426404 ($Er_4Ru_7Sb_6$), CSD-426405 ($Yb_4Ru_7Sb_6$), CSD-426406 ($Tb_4Rh_7Sb_6$), and CSD-426407 ($Er_4Rh_7Sb_6$).

Physical property measurements

Magnetic measurements were performed in the temperature range of 2.5–300 K using a Quantum Design Physical-

Table 3. Atomic coordinates and equivalent isotropic displacement parameters (pm^2) for $Er_4Ru_7Sb_6$, $Yb_4Ru_7Sb_6$, $Tb_4Rh_7Sb_6$, and $Er_4Rh_7Sb_6$. U_{eq} is defined as one third of the trace of the orthogonalized U_{ij} tensor.

Atom	Site	<i>x</i>	<i>y</i>	<i>z</i>	U_{eq}
$Er_4Ru_7Sb_6$					
Er	8 <i>c</i>	1/4	1/4	1/4	207(6)
Ru1	2 <i>a</i>	0	0	0	189(14)
Ru2	12 <i>d</i>	1/4	0	1/2	185(7)
Sb	12 <i>e</i>	0.3131(3)	0	0	184(7)
$Yb_4Ru_7Sb_6$					
Yb	8 <i>c</i>	1/4	1/4	1/4	77(1)
Ru1	2 <i>a</i>	0	0	0	56(4)
Ru2	12 <i>d</i>	1/4	0	1/2	58(2)
Sb	12 <i>e</i>	0.3123(1)	0	0	55(2)
$Tb_4Rh_7Sb_6$					
Tb	8 <i>c</i>	1/4	1/4	1/4	88(2)
Rh1	2 <i>a</i>	0	0	0	114(4)
Rh2	12 <i>d</i>	1/4	0	1/2	83(2)
Sb	12 <i>e</i>	0.3169(1)	0	0	76(2)
$Er_4Rh_7Sb_6$					
Er	8 <i>c</i>	1/4	1/4	1/4	147(2)
Rh1	2 <i>a</i>	0	0	0	163(5)
Rh2	12 <i>d</i>	1/4	0	1/2	134(3)
Sb	12 <i>e</i>	0.3160(1)	0	0	128(2)

Property-Measurement-System with magnetic flux densities up to 80 kOe (1 kOe = $7.96 \times 10^4 \text{ A m}^{-1}$). All measurements were carried out using the VSM option by packing the sample in kapton foil and attaching it to a brass sample holder. Heat capacity measurements were conducted in the temperature range of 2–300 K with samples being affixed to the pre-calibrated heat capacity puck using Apiezon N grease.

Discussion

Crystal chemistry

The antimonides $RE_4Ru_7Sb_6$ ($RE = Tb-Lu$) and $RE_4Rh_7Sb_6$ ($RE = Gd-Tm, Lu$) are 14 new mem-

$Er_4Ru_7Sb_6$			$Yb_4Ru_7Sb_6$			$Tb_4Rh_7Sb_6$			$Er_4Rh_7Sb_6$		
Er:	6	Ru2	305.5	Yb:	6	Ru2	305.1	Tb:	6	Rh2	308.3
6	Sb	310.3	6	Sb	309.8	6	Sb	313.8	6	Sb	312.2
2	Ru1	374.2	2	Ru1	373.6	2	Rh1	377.6	2	Rh1	375.9
6	Sb	270.5	Ru1:	6	Sb	269.5	Rh1:	6	Sb	276.3	Rh1:
8	Er	374.2	8	Yb	373.6	8	Tb	377.6	8	Er	375.9
Ru2:	4	Sb	269.7	Ru2:	4	Sb	269.8	Rh2:	4	Sb	270.2
4	Er	305.5	4	Yb	305.1	4	Tb	308.3	4	Er	306.9
4	Ru2	305.5	4	Ru2	305.1	4	Rh2	308.3	4	Rh2	306.9
Sb:	4	Ru2	269.7	Sb:	1	Ru1	269.5	Sb:	4	Rh2	270.2
1	Ru1	270.5	4	Ru2	269.8	1	Rh1	276.3	1	Rh1	274.3
4	Er	310.3	4	Yb	309.8	4	Tb	313.8	4	Er	312.2
1	Sb	323.0	1	Sb	323.9	1	Sb	319.4	1	Sb	319.4
4	Sb	382.6	4	Sb	381.1	4	Sb	390.8	4	Sb	387.9

Table 4. Interatomic distances (pm) for $Er_4Ru_7Sb_6$, $Yb_4Ru_7Sb_6$, $Tb_4Rh_7Sb_6$, and $Er_4Rh_7Sb_6$ calculated with the powder lattice parameters. Standard deviations are equal or smaller than 0.2 pm. All distances of the first coordination spheres are listed.

bers with the cubic $U_4Re_7Si_6$ -type structure [25]. The intermediate-valent ytterbium compound $Yb_4Rh_7Sb_6$ has been reported earlier [22, 26]. So far, more than 50 silicides, germanides, and germanide gallides [21, 27–41] with this cubic structure type have been reported. Especially the uranium-containing phases were studied in detail with respect to the magnetic ground state of uranium, *e. g.* the 25 K anti-ferromagnet $U_4Tc_7Si_6$ [37] or the 6.8 K ferromagnet $U_4Ru_7Ge_6$ [32, 36]. Besides the many tetrelides, only the pnictides $Mg_4Rh_7P_6$, $Mg_4Rh_7As_6$, $Mg_4Ir_7As_6$, $Yb_4Rh_7As_6$ [42], $U_4Ru_7As_6$ [43], and $Yb_4Rh_7Sb_6$ [22, 26] are known. The present series of ternary ruthenium and rhodium antimonides extends the family of $U_4Re_7Si_6$ -type intermetallics. Similar to the series of silicides and germanides, also the antimonides are formed only with the smaller rare earth elements. In agreement with the lanthanoid contraction, we observed a decrease of the cell volume from the gadolinium to the lutetium compound. Only $Yb_4Ru_7Sb_6$ and $Yb_4Rh_7Sb_6$ show small positive deviations from this plot as a consequence of their intermediate ytterbium valence (*vide infra*).

As an example we discuss the $Er_4Ru_7Sb_6$ structure herein. A view of this structure approximately along

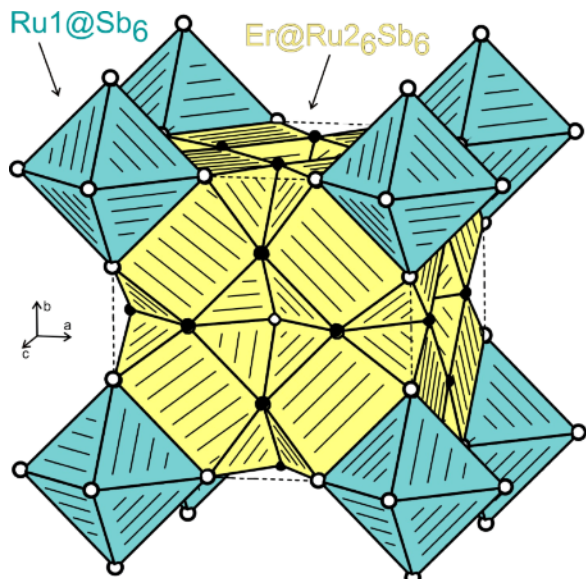


Fig. 1 (color online). The crystal structure of $Er_4Ru_7Sb_6$. Erbium, ruthenium and antimony atoms are drawn as medium grey, black filled and open circles, respectively. The condensation pattern of $Ru1@Sb6$ octahedra and $Er@Ru2_6Sb6$ cuboctahedra is emphasized.

the c axis is given in Fig. 1. The shortest interatomic distances in the $Er_4Ru_7Sb_6$ structure occur between the ruthenium and antimony atoms, *i. e.* 271 pm Ru1–Sb and 270 pm Ru2–Sb, only slightly longer than the sum of the covalent radii of 265 pm [44]. The Ru1 atoms have six antimony neighbors in octahedral coordination while the Ru2 atoms have only four closer antimony atoms in strongly flattened tetrahedral coordination. The octahedral building units are similar to those in the skutterudites $SrRu_4Sb_{12}$ (262 pm Ru–Sb) and $BaRu_4Sb_{12}$ (263 pm Ru–Sb) [45].

Usually, the 4-7-6 structures have been described by a condensation of the octahedral and flattened tetrahedral units [21, 28]. An alternative, very easy description is possible with $Ru1@Sb6$ octahedra and slightly distorted $Er@Ru2_6Sb6$ cuboctahedra (Fig. 1) as building units. The octahedra show a *bcc* packing, and every octant of the cubic cell is filled with the cuboctahedra. The latter are condensed *via* all six trapezoidal faces. This substructure automatically leaves the octahedral antimony voids for the Ru1 atoms.

The Ru2 atoms show Ru2–Ru2 distances of 306 pm, distinctly longer than in *hcp* ruthenium (6 \times 265 and 6 \times 271 pm) [46]. These interactions are probably quite weak.

Magnetic properties

The antimonides $RE_4Ru_7Sb_6$ with $RE = Dy-Lu$ have been obtained in X-ray-pure form and they were studied with respect to their magnetic properties. The rhodium-containing samples showed small amounts of the binary rare earth antimonides $RESb$ as by-products. Therefore, no susceptibility studies of these samples were carried out.

The temperature dependence of the magnetic susceptibilities (χ and χ^{-1} data) of $Dy_4Ru_7Sb_6$, $Ho_4Ru_7Sb_6$, and $Er_4Ru_7Sb_6$ measured at an applied field of 10 kOe are displayed in Figs. 2a–4a (insets depict measurements of the respective compounds measured in zero-field-cooled/field-cooled mode (ZFC/FC) with an applied field of 100 Oe). The Dy and Ho compounds exhibit antiferromagnetic ordering at the Néel temperatures of $T_N = 10.1(5)$ and 5.1(5) K, respectively, clearly discernable from their χ data as well as the spin reorientation at very low temperatures. The antiferromagnetic ordering is also evident from the specific heat data. In case of the Er compound only the ZFC/FC measurement pointed

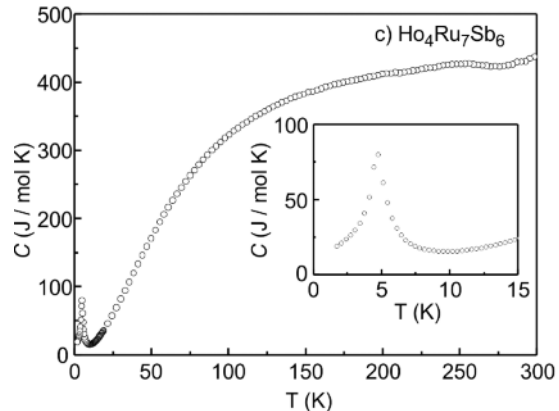
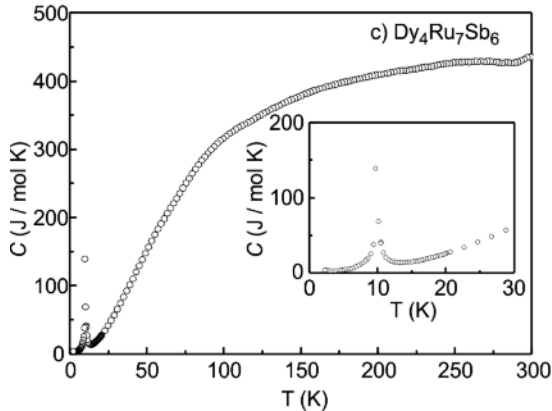
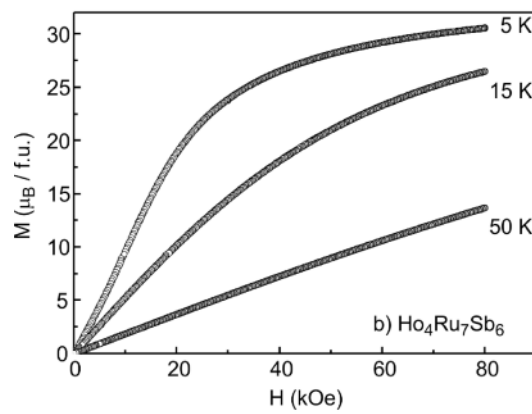
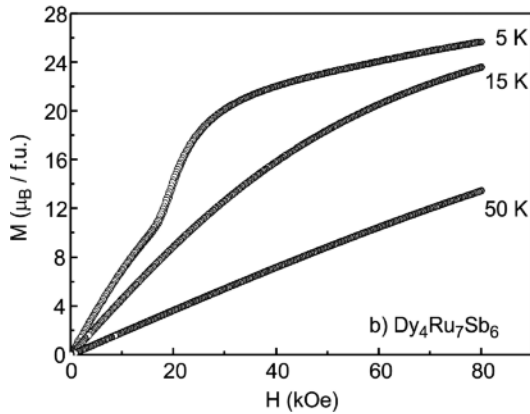
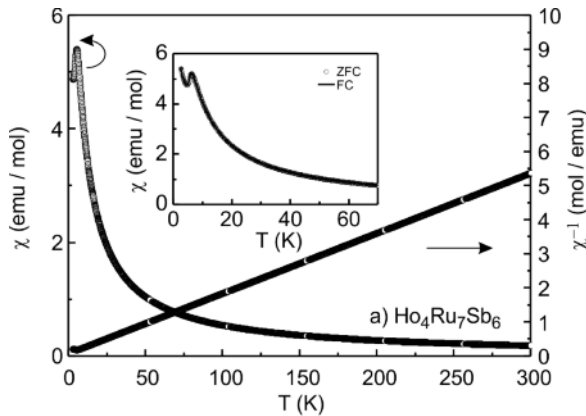
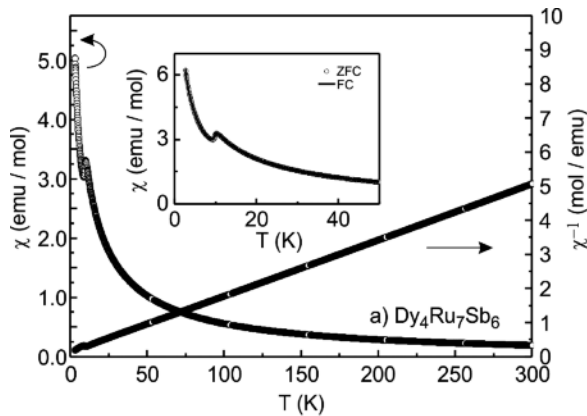


Fig. 2. (a) Temperature dependence of the magnetic susceptibility (χ and χ^{-1} data) of $Dy_4Ru_7Sb_6$ measured at an applied field of 10 kOe. The low-temperature behavior in zero-field-cooled/field-cooled mode with an applied field of 100 Oe is depicted in the inset; (b) magnetization isotherms of $Dy_4Ru_7Sb_6$ at 5, 15, and 50 K; (c) temperature dependence of the specific heat of $Dy_4Ru_7Sb_6$ measured in zero magnetic field.

Fig. 3. (a) Temperature dependence of the magnetic susceptibility (χ and χ^{-1} data) of $Ho_4Ru_7Sb_6$ measured at an applied field of 10 kOe. The low-temperature behavior in zero-field-cooled/field-cooled mode with an applied field of 100 Oe is depicted in the inset; (b) magnetization isotherms of $Ho_4Ru_7Sb_6$ at 5, 15, and 50 K; (c) temperature dependence of the specific heat of $Ho_4Ru_7Sb_6$ measured in zero magnetic field.

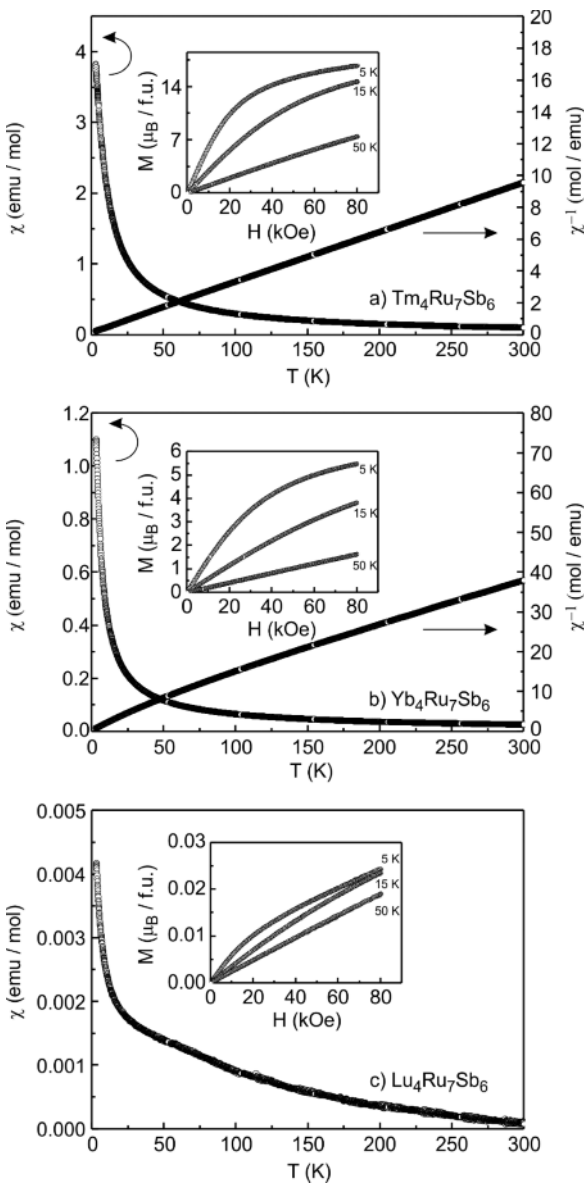
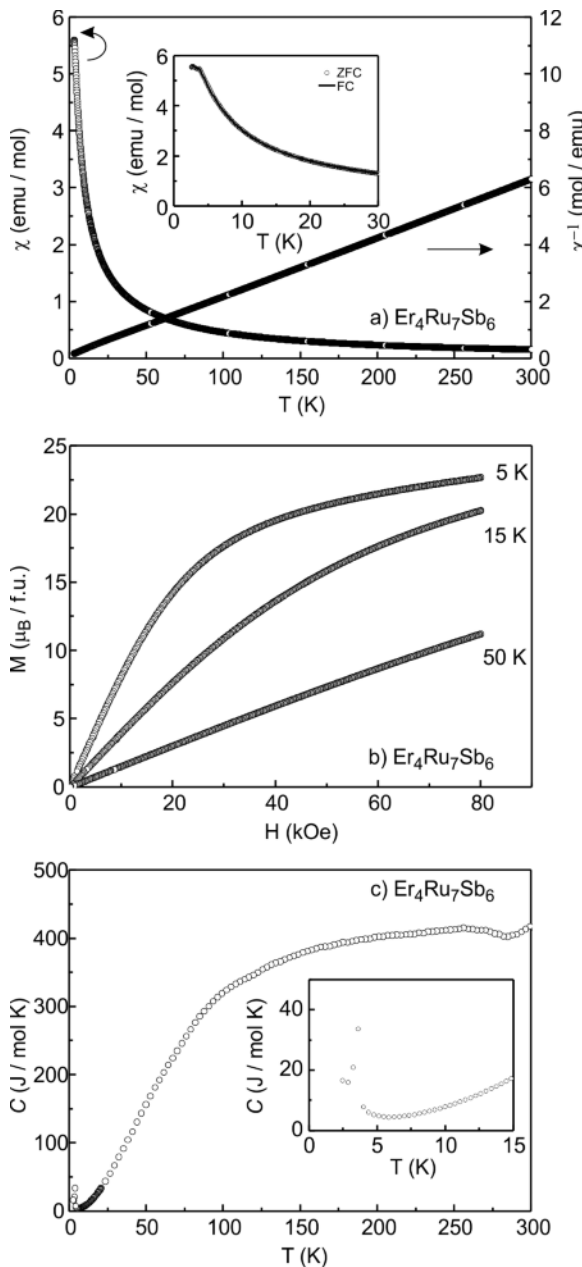


Table 5. Magnetic properties of ternary antimonides $RE_4T_7Sb_6$: μ_{exp} , experimental magnetic moment; μ_{eff} , effective magnetic moment; θ_P , paramagnetic Curie temperature; μ_{sm} , experimental saturation magnetization; $\mu_{\text{sm(calc)}}$, calculated saturation magnetization; T_N , Néel temperature.

Compound	μ_{exp} (μ_B / RE)	μ_{eff} (μ_B / RE)	θ_P (K)	μ_{sm} (μ_B / fu)	$\mu_{\text{sm(calc)}}$ (μ_B / fu)	T_N (K)
Dy ₄ Ru ₇ Sb ₆	11.0(1)	10.65	-8.9(5)	25.7(1)	40.0	10.0(5)
Ho ₄ Ru ₇ Sb ₆	10.7(1)	10.61	-4.2(5)	30.6(1)	40.0	5.1(5)
Er ₄ Ru ₇ Sb ₆	9.9(1)	9.58	-6.5(5)	22.7(1)	36.0	4.0(5)
Tm ₄ Ru ₇ Sb ₆	8.1(1)	7.56	-6.5(5)	16.8(1)	28.0	-

towards antiferromagnetic ordering (inset of Fig. 4a). We therefore conducted heat capacity measurements (2–300 K) in order to determine the proper ordering temperature of $T_N = 4.0(5)$ K. No magnetic ordering was evident for the thulium, ytterbium and lutetium compound.

The inverse susceptibilities of $RE_4Ru_7Sb_6$ ($RE = Dy, Ho, Er, Tm$) could be fitted with the Curie-Weiss law in the temperature ranges 20–300 K, yielding the experimental values listed in Table 5. The magnetic moments are close to the values of the free RE^{3+} ions. The Weiss constants are negative. This is indicative of antiferromagnetic interactions.

Figs. 2b–4b show the magnetization isotherms of $RE_4Ru_7Sb_6$ ($RE = Dy, Ho, Er, Tm$) measured at 5, 15 and 50 K. As expected for paramagnetic materials, the isotherms show close to linear increase in magnetization with the applied field at 50 K. The isotherms of the Dy and Ho compounds at 5 K exhibit s-like curvatures due to spin reorientations at critical fields of 20 and 10 kOe, respectively. The other two compounds show a tendency of saturation at high fields in the form of a typical Brillouin function. At 5 K and the highest obtainable field of 80 kOe the magnetization values reached between 60 and 76 % of the theoretical values, a consequence of the polycrystalline character of our samples.

The inverse susceptibility of Yb₄Ru₇Sb₆ shows a weak curvature over the whole temperature range, similar to isotropic Yb₄Rh₇Sb₆ [22]. The data could be fitted in the temperature range of 30–300 K with the modified Curie-Weiss law $\chi = \chi_0 + (C/(T - \theta_P))$, resulting in a magnetic moment $\mu_{\text{eff}} = 3.71(1)$ μ_B per Yb atom and a negative Weiss constant of $\theta_P = -11.0(5)$ K. The experimental magnetic moment differs significantly from the data of the theoretical free ion, spin only, value of 4.54 μ_B per Yb³⁺ and points toward an intermediate valence state of ytterbium. This is also evident from the small magnetization value of 5.5(1) μ_B per formula unit (fu) at 5 K and 80 kOe which is much smaller than the theoretical value of 16 μ_B .

Lu₄Ru₇Sb₆ shows much smaller susceptibility values since the Lu³⁺ cation with filled 4f shell is diamagnetic. The absolute values at room temperature are compatible with Pauli paramagnetism. The increase of the susceptibility towards lower temperatures is due to minor amounts of paramagnetic impurities. Also the magnetization values are two orders of magnitude lower than those of the paramagnetic ones.

Acknowledgement

This work was supported by the Deutsche Forschungsgemeinschaft through SPP 1458 *Hochtemperatursupraleitung in Eisenpnictiden*.

- [1] M. Rotter, M. Tegel, D. Johrendt, *Phys. Rev. Lett.* **2008**, *101*, 107006.
- [2] M. Rotter, M. Pangerl, M. Tegel, D. Johrendt, *Angew. Chem. Int. Ed.* **2008**, *47*, 7949.
- [3] D. C. Johnston, *Adv. Phys.* **2010**, *59*, 803.
- [4] D. Johrendt, H. Hosono, R.-D. Hoffmann, R. Pöttgen, *Z. Kristallogr.* **2011**, *226*, 435.
- [5] D. Kußmann, R. Pöttgen, U. Ch. Rodewald, C. Rosenhahn, B. D. Mosel, G. Kotzyba, B. Künnen, *Z. Naturforsch.* **1999**, *54b*, 1155.
- [6] P. Villars, K. Cenzual, *Pearson's Crystal Data: Crystal Structure Database for Inorganic Compounds* (release 2009/10), ASM International®, Materials Park, Ohio, **2009**.
- [7] A. Szytuła, J. Leciejewicz, *Handbook of Crystal Structures and Magnetic Properties of Rare Earth Intermetallics*. CRC Press, Boca Raton, **1994**.
- [8] R. A. Gordon, F. J. DiSalvo, R. Pöttgen, *J. Alloys Compd.* **1995**, *228*, 16.

- [9] I. Schellenberg, R.-D. Hoffmann, S. Seidel, C. Schwickerert, R. Pöttgen, *Z. Naturforsch.* **2011**, *66b*, 985.
- [10] R. Pöttgen, *Z. Naturforsch.* **1995**, *50b*, 175.
- [11] Yu. Grin, M. Ellner, B. Predel, K. Peters, *J. Alloys Compd.* **1993**, *201*, 209.
- [12] M. L. Fornasini, P. Manfrinetti, D. Mazzone, P. Riani, G. Zanicchi, *J. Solid State Chem.* **2004**, *177*, 1919.
- [13] I. Schellenberg, R.-D. Hoffmann, C. Schwickerert, R. Pöttgen, *Solid State Sci.* **2011**, *13*, 1740.
- [14] A. Löhken, A. Mewis, *Z. Anorg. Allg. Chem.* **2004**, *630*, 2418.
- [15] U. Pfannenschmidt, D. Johrendt, F. Behrends, H. Eckert, M. Eul, R. Pöttgen, *Inorg. Chem.* **2011**, *50*, 3044.
- [16] I. Schellenberg, M. Eul, R. Pöttgen, *Z. Naturforsch.* **2010**, *65b*, 18.
- [17] K. Schäfer, W. Hermes, U.Ch. Rodewald, R.-D. Hoffmann, R. Pöttgen, *Z. Naturforsch.* **2011**, *66b*, 777.
- [18] R. Pöttgen, Th. Gulden, A. Simon, *GIT Labor-Fachzeitschrift* **1999**, *43*, 133.
- [19] D. Niepmann, Yu. M. Prots', R. Pöttgen, W. Jeitschko, *J. Solid State Chem.* **2000**, *154*, 329.
- [20] K. Yvon, W. Jeitschko, E. Parthé, *J. Appl. Crystallogr.* **1977**, *10*, 73.
- [21] B. Heying, K. Katoh, Y. Niide, A. Ochiai, R. Pöttgen, *Z. Anorg. Allg. Chem.* **2004**, *630*, 1423.
- [22] I. Schellenberg, M. Eul, R. Pöttgen, *Z. Kristallogr.* **2010**, *225*, 339.
- [23] G. M. Sheldrick, SHELXL-97, Program for the Refinement of Crystal Structures, University of Göttingen, Göttingen (Germany) **1997**.
- [24] G. M. Sheldrick, *Acta Crystallogr.* **2008**, *A64*, 112.
- [25] L. G. Akselrud, Y. P. Yarmolyuk, E. I. Gladyshevskii, *Dopov. Akad Nauk Ukr. RSR, Ser. A* **1978**, 359.
- [26] A. Leithe-Jasper, R. Cardoso-Gil, R. Ramlau, U. Burkhardt, *Z. Kristallogr. NCS* **2006**, *221*, 255.
- [27] A. I. Zyubrik, R. R. Olenych, Y. P. Yarmolyuk, *Dopov. Akad. Nauk Ukr. RSR (Ser. A)* **1982**, 74.
- [28] N. Engel, B. Chabot, E. Parthé, *J. Less-Common Met.* **1984**, *96*, 291.
- [29] M. Francois, G. Venturini, J. F. Marêché, B. Malaman, B. Roques, *J. Less-Common Met.* **1985**, *113*, 231.
- [30] R. R. Olenych, Y. P. Yarmolyuk, *Visn. Lviv Derzh. Univ. (Ser. Khim.)* **1986**, *27*, 47.
- [31] R. R. Olenych, Y. P. Yarmolyuk, R. V. Skokozdne, *Ukr. Fiz. Zh. Russ. Ed.* **1987**, *32*, 615.
- [32] B. Lloret, B. Buffat, B. Chevalier, J. Etourneau, *J. Magn. Magn. Mater.* **1987**, *67*, 232.
- [33] A. A. Menovsky, *J. Magn. Magn. Mater.* **1988**, *76&77*, 631.
- [34] Y. Dalichaouch, M. B. Maple, M. S. Torikachvili, A. L. Giorgi, *Phys. Rev. B* **1989**, *39*, 2423.
- [35] B. Y. Kotur, R. I. Andrusyak, *Inorg. Mater.* **1991**, *27*, 1207.
- [36] S. A. M. Mentink, G. J. Nieuwenhuys, A. A. Menovsky, J. A. Mydosh, *J. Appl. Phys.* **1991**, *69*, 5484.
- [37] F. Wastin, J. Rebizant, J. P. Sanchez, A. Blaise, J. Goffart, J. C. Spirlet, C. T. Walker, F. Fuger, *J. Alloys Compd.* **1994**, *210*, 83.
- [38] A. V. Morozkin, I. A. Sviridov, *J. Alloys Compd.* **2000**, *296*, L4.
- [39] M. A. Zhuravleva, X. Wang, A. J. Schultz, T. Bakas, M. G. Kanatzidis, *Inorg. Chem.* **2002**, *41*, 6056.
- [40] K. Katoh, H. Abe, D. Negishi, G. Terui, Y. Niide, A. Ochiai, *J. Magn. Magn. Mater.* **2004**, *279*, 118.
- [41] T. Eriksson, P. Nordblad, Y. Andersson, *J. Solid State Chem.* **2005**, *178*, 1495.
- [42] A. Wurth, A. Löhken, A. Mewis, *Z. Anorg. Allg. Chem.* **2001**, *627*, 1213.
- [43] H. Noël, M. Potel, D. Kaczorowski, *J. Alloys Compd.* **2000**, *302*, L1.
- [44] J. Emsley, *The Elements*, Oxford University Press, Oxford **1999**.
- [45] C. B. H. Evers, L. Boonk, W. Jeitschko, *Z. Anorg. Allg. Chem.* **1994**, *620*, 1028.
- [46] J. Donohue, *The Structures of the Elements*, Wiley, New York **1974**.